Polar Cluster-Based Target Tracking for Maritime Radar Applications

Lucas Paes Moreira, Michailas Romanovas
Institute of Communications and Navigation
German Aerospace Center (DLR)
Neustrelitz, Germany
{lucas.paesmoreira, michailas.romanovas}@dlr.de

Abstract—Accurate maritime situational awareness is essential for safety, security, and environmental protection. While the Automatic Identification System (AIS) is widely used, it is vulnerable to spoofing and intentional manipulation. These limitations can be mitigated through independent validation using marine X-band radar, where high-resolution coastal sensors detect extended targets with distance-dependent sparsity and data in polar coordinates.

This paper evaluates a polar-domain clustering algorithm and its impact on extended-object multi-target tracking (MTT) algorithms, evaluating in several frameworks of different complex. A Random Matrix Model (RMM) incorporating radar intensity improves estimation of target centroid and extent, enhancing vessel shape representation compared to spatial-only approaches.

Performance is validated on real-world X-band radar data within selected Regions of Interest (ROI) and different distances from the sensor, where objects have different point cloud spatial densities. Results show that data clustering in polar domain is more robust against the distance variability of detections w.r.t. the sensor and benefits the tracking algorithms performance.

Index Terms—polar clustering, extended objects, multiple target tracking, radar tracking, maritime surveillance

I. Introduction

Maritime monitoring is essential for ensuring the safety, security, and efficiency of global trade, particularly in congested areas such as ports and harbors. The growing interest in autonomous maritime operations further increases the demand for reliable, real-time data, typically achieved through multi-sensor integration for navigation and route planning.

Automatic Identification System (AIS) data, although widely used, is vulnerable to manipulation and interference from Global Navigation Satellite System (GNSS) jamming and spoofing [1]. These limitations highlight the need for complementary, independent sensing systems. X-band marine radar provides an important and in many locations already existing alternative, enabling the detection of non-cooperative targets and ensuring robust monitoring even in GNSS-denied environments.

Recent advances in Multiple Target Tracking (MTT) have significantly improved maritime surveillance, particularly through Extended Object Tracking (EOT) methods. Unlike point-target models, EOT exploits the fact that modern high-resolution radars produce multiple detections per object, enabling the estimation of both kinematic states and object extent. The Random Matrix Model (RMM) [2], [3] is a well-established and well-understood approach, representing target extent as an ellipse while capturing uncertainties in both kinematic and geometric parameters within a probabilistic framework.

Extended objects generate multiple detections, forming point clouds rather than single measurements. Clustering algorithms group spatially and temporally consistent detections, treating each cluster as a single measurement. Within the RMM framework, the cluster centroid provides the target position, while the scatter matrix describes its extent and orientation, commonly modeled using an Inverse Wishart distribution [3]. Fig. 1 illustrates a large vessel detected by a X-band radar, with its estimated position and extension.

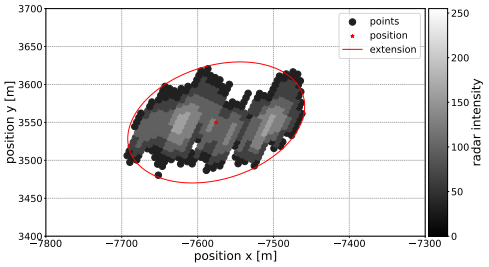

Fig. 1: Example for X-band radar detections for a large vessel with the intensity information and an ellipse approximation.

Marine X-band radar data are typically acquired in polar coordinates (range and azimuth), but are often transformed into Cartesian coordinates for processing [4], [5]. This transformation introduces non-uniformities in measurement density due to the radar's angular resolution: distant targets yield sparse point clouds, while closer targets produce denser measurements. Such variability complicates clustering and tracking, particularly over large observation ranges, where Cartesian representations may also introduce distortions and increased computational costs.

To address these challenges, this work proposes a clustering approach directly in the polar domain. By preserving the radar's native geometry, this method enables more consistent clustering across varying ranges and

avoids the need for computationally expensive coordinate transformations.

The proposed clustering method generates extended-object measurements from X-band radar data, which are subsequently evaluated using different MTT frameworks, including Sequential Probability Ratio Test (SPRT), Joint Integrated Probabilistic Data Association (JIPDA), and Probability Hypothesis Density (PHD) filters.

II. Methods

Raw radar data provides detections in the polar coordinate plane (range r and azimuth ϕ). We define the set of raw detections at time k as $\mathcal{Z}_k = \{\mathbf{z}_k^i\}_{i=1}^{N_k}$, where N_k is the total number of detections and each individual measurement is $\mathbf{z}_k^i = [r_k^i, \phi_k^i]^T$. These measurements constitute point clouds that may originate from true targets, Aids to Navigation (AtoN), static infrastructure, or clutter. To associate detections with their respective sources, a clustering algorithm is applied to $\mathcal{Z}_k$. Assuming each cluster originates from an independent source, they can be processed independently in the successive steps of the tracking pipeline. Considering the spatial 2D nature of radar detections, and the usual representation of target states in Cartesian domain, the most common approach is to map the detections into Cartesian domain before clustering, using standard trigonometric conversion:

$$\mathbf{z}_k^i = \begin{bmatrix} p_{x,k}^i \\ p_{y,k}^i \end{bmatrix} = \begin{bmatrix} r_k^i \cos\phi_k^i \\ r_k^i \sin\phi_k^i \end{bmatrix} \tag{1}$$

where $p_{j,k}^i$ represents the Cartesian position component in dimension $j \in \{x, y\}$.

There are numerous algorithms for generic clustering task, including K-means, Gaussian Mixture Models (GMM), and Density-Based Spatial Clustering of Applications with Noise (DBSCAN). While each has trade-offs, DBSCAN is the mostly adopted in the literature and particularly effective in radar data, being also applied in the X-band maritime domain [6], suggesting a suitable starting point. Nevertheless, density-based algorithms, such as DBSCAN, rely on the distance between detections for assigning them to the same cluster, i.e. $d(\mathbf{z}_k^i, \mathbf{z}_k^j) \leqslant \varepsilon$ for $i \neq j$ and $\mathbf{z}_k^i, \mathbf{z}_k^j \in \mathcal{Z}_k$, where ε is a hyper-parameter of the algorithm.

Considering the range-dependence behavior of clusters density in Cartesian domain, tuning a generic single hyper-parameter is unfeasible for long-range resolution sensors. To tackle this issue, adaptive DBSCAN algorithms are proposed [7], [8], however, these approaches require more computational resources and the implementation of a custom algorithm instead of stable versions publicly available.

An alternative approach is to perform the clustering directly in polar domain. This approach is particularly suitable for rotational marine radars, which have relatively constant range and azimuth sensor resolutions, i.e. the distance between two neighbor points in azimuth do not vary with respect to the range value. In order to perform the clustering in this domain, it is important to note that the angular component (azimuth) is defined on S^1, hence, all distance measures and processing steps must respect its circular topology and inherent 2π-periodicity. One proposed solution for this problem is to convert the polar points in a cylindrical coordinate system [9]. In this proposed system, all points are mapped from the polar coordinates to the lateral surface of a cylinder, i.e. given a polar point $\mathbf{z}(r, \phi)$:

$$\mathbf{z}(r, \phi) \rightarrow \mathbf{z}(x, y, z) = \begin{bmatrix} R\cos\phi \\ R\sin\phi \\ r \end{bmatrix}, \tag{2}$$

where R is the radius of the base circle of the cylinder. Here R can be also seen as a scale parameter that can be adjusted based on the weights (importance) of difference in r and ϕ, greater R indicates the difference observed in ϕ is more important than r. Thus, any point (x', y') on the rectangular space (X', Y'), with $X' \backsim R\phi$ and $Y' \backsim r$, can be written as,

$$(x', y') = (f(\phi), r) = (R\phi, r). \tag{3}$$

Fig. 2 illustrates the reconstruction of polar coordinates on the rectangular plane (X', Y') using cylindrical coordinates described above, adapted from [9]. On the left, the coordinates with the azimuth values represented by the angle in the cylinder base on the (X, Y) plane, and the range values represented in the height of the cylinder, the radius R is the scaling factor between range and azimuth values. Here two polar points A and B are located in the lateral surface and the distance between them represented by the orange line. On the right, the mapping of the points in the unwrapped lateral surface where azimuth values are in the X' axis and range values are in the Y' axis, showing the two possible distances between the points, $d(A, B1)$ and $d(A, B2)$, as a consequence of angle values circularity.

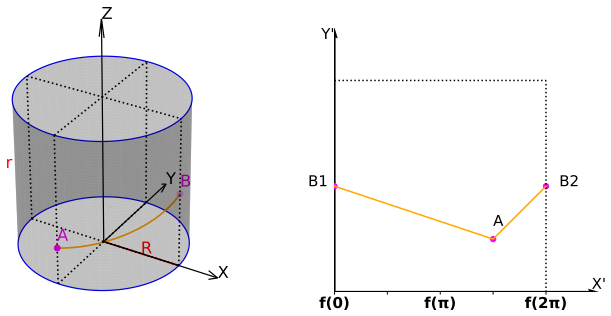

Fig. 2: Reconstruction of polar coordinates on the rectangular plane (X', Y') using cylindrical coordinates.

After mapping points to the lateral surface of the cylinder with above equation, the distance between two points on the lateral surface (i.e., geodesic) can be estimated as similar to Euclidean distance,

$$d(\mathbf{z}_k^i, \mathbf{z}_k^j) = \left[(r_k^i - r_k^j)^2 + R^2(\phi_k^i - \phi_k^j)^2\right]^{\frac{1}{2}}. \tag{4}$$

The above distance, however, has as unit a non-linear combination of meters and radians with no direct physical interpretation. Despite the mathematical correctness, this unit imposes challenges on defining (and interpreting) the distance hyper-parameter ε. An easy fix is to define $R = \sigma_r/\sigma_\phi$, where σ_r and σ_ϕ are the sensor resolution in range and azimuth respectively. This approach not only maps the distance $d(\mathbf{z}_k^i, \mathbf{z}_k^j)$ to meters, but also properly scales the weights of each difference based on its respective sensor resolution, removing R as an additional clustering hyper-parameter to be tuned by the user.

Radar data used in this work are recorded in ASTERIX CAT240 protocol [10], where each radar reflection is represented as a 2D cell in polar coordinates, with the corner values r_{start} and r_{end} in the range dimension and ϕ_{start} and ϕ_{end} in the azimuth dimension. Thus, the sensor resolution can be inferred by the detection cell size, for instance $\sigma_r = r_{\text{end}} - r_{\text{start}}$ and $\sigma_\phi = \phi_{\text{end}} - \phi_{\text{start}}$. It is important to note that the values provided by the data in CAT240 protocol not necessarily represent the physical sensor resolution, but only provide a simple heuristic for the scale factor R. Additionally, the angle difference must be properly implemented in S^1, which can be easily accomplished using the two-argument four-quadrant arctan, named arctan2, which returns a signed angle difference in the range $-\pi \leqslant \phi_{\text{diff}} < \pi$, and it is available in most current programming languages. The custom distance (4), using $R = \sigma_r/\sigma_\phi$ and $\phi_k^i - \phi_k^j = \text{arctan2}(\phi_k^i - \phi_k^j)$, is then used in the clustering algorithm.

The design of parametric MTT algorithm involves two key components. First, a state and extent estimator, typically based on Kalman-filter-like algorithm, which recursively estimates the kinematic and geometric properties of a target from noisy, target-associated measurements. Second, the MTT architecture which governs hypothesis generation, data association, and track management over time.

All considered trackers employ the RMM [2], where the kinematic state $\mathbf{x}_k$ follows a Gaussian distribution and the target extent $\mathbf{X}_k$ is modeled as an IW distribution. This formulation enables joint estimation of position, velocity, and object shape.

In contrast to the classical RMM, we compute intensity-weighted cluster statistics:

$$\bar{\mathbf{z}}_k^w = \frac{\sum_i l_k^i \mathbf{z}_k^i}{\sum_i l_k^i}, \tag{5}$$

$$\bar{\mathbf{Z}}_k^w = \frac{n_k}{\sum_i l_k^i} \sum_i l_k^i (\mathbf{z}_k^i - \bar{\mathbf{z}}_k^w)(\mathbf{z}_k^i - \bar{\mathbf{z}}_k^w)^T. \tag{6}$$

This preserves the physical interpretation of n_k as the number of measurements while biasing the estimate toward strong reflections.

At steady state, the extension estimate satisfies

$$\mathbf{X}_{\infty,k} = \frac{1}{\rho}\left(\frac{\bar{\mathbf{Z}}_k}{n_k} - \mathbf{R}_k\right), \tag{7}$$

which is also used for initializing new tracks from unassociated clusters. Target motion is described by a linear constant velocity motion model in 2D.

For the hypothesis generation and data association step, we consider several MTT formulations of increasing complexity. As a baseline, the Sequential Probability Ratio Test (SPRT) tracker [11] performs hard assignments and updates track existence using available statistics on detection probability P_D, probability of false alarm P_{FA}, and the gate probability P_G. Since spatial likelihoods (in our case both kinematic and shape) do not affect existence updates, this approach is effective primarily in low-clutter scenarios with well-separated targets.

To handle ambiguous associations, we adopt the Joint Probabilistic Data Association (JPDA) framework [12], [13]. JPDA evaluates all feasible joint association events χ and computes their posterior probabilities $p(\chi|Z^k)$. The marginal association weights

$$\beta_j^t = \sum_\chi p(\chi|Z^k)\, \hat{\omega}_{jt}(\chi), \quad \beta_0^t = 1 - \sum_j \beta_j^t, \tag{8}$$

are used for soft updates, improving robustness in dense environments. The Joint Integrated PDA (JIPDA) [14] further introduces a probabilistic track existence variable, where the existence probability is updated jointly with association hypotheses. This provides a principled track quality measure and unifies estimation and track management.

As an additional comparison, we include a multi-instance IPDA [15], running multiple instances of single-object IPDA estimators connected via greedy implementation of multiple local nearest neighbor associations.

Finally, we consider a cluster-based Gaussian Inverse Wishart PHD (CB-GIW-PHD) filter suggested in [16]. The multi-target posterior is approximated by a mixture of GIW components, where each component represents a potential object. In contrast to classical extended-object PHD filters, we directly process pre-clustered measurements, thereby avoiding combinatorial partitioning.

All the algorithms above (except of SPRT) are operating on spatial likelihood to be input in the hypothesis generation methods. Standard point-target formulations (point reflection measurement likelihood) are not directly applicable to high-resolution radar, as the clutter likelihood $\lambda_c^{n_k}$ leads to excessive penalization for large clusters. To address this, each cluster Z_j is treated as a single observation in the cluster likelihood formulation.

A naive likelihood formulation based on centroid and shape densities leads to numerical imbalance due to the concentration of the Wishart distribution for large n_k. We therefore define a normalized cluster likelihood via a ratio:

$$\Lambda(Z_j) = \frac{1}{P_G} \frac{p(\bar{\mathbf{z}}_j|H_1)\, p(\bar{\mathbf{Z}}_j|H_1)}{\lambda_c\, p(\bar{\mathbf{Z}}_j|H_0)}. \tag{9}$$

Both target and clutter shape terms are modeled as Wishart distributions,

$$p(\bar{\mathbf{Z}}_j|H_i) = \mathcal{W}_d(\bar{\mathbf{Z}}_j; n_k - 1, \mathbf{V}_i), \tag{10}$$

with $\mathbf{V}_1$ given by the predicted extent and $\mathbf{V}_0$ representing a broad clutter model. This formulation stabilizes likelihood ratios while preserving sensitivity to geometric structure.

To further improve robustness, we decouple estimation and gating. The innovation covariance for state updates scales with cluster size,

$$\mathbf{S}_{k|k-1} = \mathbf{H}\mathbf{P}_{k|k-1}\mathbf{H}^T + \frac{\rho\mathbf{X}_{k|k-1} + \mathbf{R}_k}{n_k}, \tag{11}$$

while the validation gate uses the full extent:

$$\mathbf{S}_{k,\text{gate}} = \mathbf{H}\mathbf{P}_{k|k-1}\mathbf{H}^T + \rho\mathbf{X}_{k|k-1} + \mathbf{R}_k. \tag{12}$$

All likelihood computations are carried out in the log-domain using the Log-Sum-Exp identity to avoid numerical underflow in PDA and PHD modules. As SPRT does not use likelihoods, there it is not relevant.

On the track management step, detection and clutter are assumed constant within the region of interest, with $P_D = 0.8$ and $\lambda_c = 10^{-4}$. The SPRT tracker uses $P_{FA} = 0.01$, while the PHD filter applies a survival probability $P_S = 0.95$.

Track initiation is performed from unassociated clusters, with positions initialized from measurements, zero velocity, and inflated covariance. Existence probabilities are initialized at 0.6 for (J)IPDA-based trackers, while PHD components are assigned small initial weights. Extensions are initialized using steady-state approximations with fixed and low value of degrees of freedom to allow easier extension adjustment in subsequent estimation steps.

Data association is implemented using a greedy M:N assignment strategy for JIPDA and PHD, 1:N to IPDA and 1:1 for SPRT trackers, prioritizing computational efficiency over optimality.

Tracks are pruned based on existence probability, kinematic uncertainty, missed detections, and extension uncertainty for SPRT, IPDA and JIPDA versions. For PHD, pruning is weight-based, complemented by a merging step that combines nearby components using moment matching [17]. Identity consistency is maintained by an additional step, retaining the dominant component label after merging. Generic PHD tracker does not include ID management and this shall be added on top, as ID preservation is extremely important in maritime applications.

III. Results

The evaluation of above-mentioned methods was performed using a real-world marine radar data set. The data was recorded by a static radar station located in the Baltic Sea with a sensor that can detect signal reflections up to 30 km. Two scenarios were selected, one close to the sensor with distance up to 5 km (near-field) and a scenario with distances higher than 20 km (far-field). This data set was manually labeled for a one-hour period, annotating pixels of objects of interest, for instance cooperative vessels (confirmed by AIS messages), non-cooperative vessels (without AIS) and Aid-to-Navigation (AtoN) devices, e.g. maritime buoys. These labels were then used as ground-truth for all analysis. In order to compare the methods in both scenarios, near and far field, two subsets were created, one for each ROI.

The density-based clustering algorithm is heavily sensitive to the main hyper-parameters, i.e. the ε and minimum number of points, therefore a grid-search was performed with a collection of possible values for each parameter. In order to benchmark against the proposed approach in polar domain, the clustering in Cartesian domain using standard trigonometric functions was evaluated. The outputs from the clustering algorithm are evaluated using the Adjusted Rand Index (ARI) [18] and the difference between the number of clusters (labeled and estimated) for each data frame. The combination of both metrics, with larger ARI and lower cluster count difference, were used to define the optimal hyper-parameter combination.

The proposed trackers were evaluated using the classical OSPA [19] and the T-GOSPA [20] metrics. The latter was used to provide a performance measure for the ID switch, which cannot be deduced from OSPA metric. These metrics were computed in the near-field and far-field scenarios with the same set of clustering hyper-parameters suitable for both, for instance $\varepsilon = 55$ and a minimum sample of 3. For OSPA, the metrics (overall distance, accuracy and cardinality) were computed per frame while T-GOSPA returns its metrics as a set of scalars, representing the performance for the entire period of time, from which it was taken the ID switch, to complement the results provided by OSPA. Fig. 3 shows the OSPA results per time step for all trackers with measurements formed by clusters in Cartesian and polar domains in the near-field scenario. Similarly, Fig. 4 shows the OSPA results for the far-field scenario. The track switching costs from T-GOSPA are shown in Table. I for both scenarios and clustering domains.

The results in Fig. 3 show the same performance for both clustering domains, considering that the clusters point clouds are well-formed, clearly separated, have high spatial density, and the polar to Cartesian mapping error is negligible for shorter ranges. For this reason, the localization error, given by OSPA's accuracy, is low for all trackers. The high variation on cardinalities are artifacts from the combination of two factors, the frequent object occlusion, and the use of data labels as reference for the metrics. When the occlusion occurs, there is no measurement associated to the object, therefore no labels are available, however the tracks are persistent for a limited period of time for all trackers, resulting in a false positive. This imposes a challenging assessment purely on metrics as false positives can penalize an intended

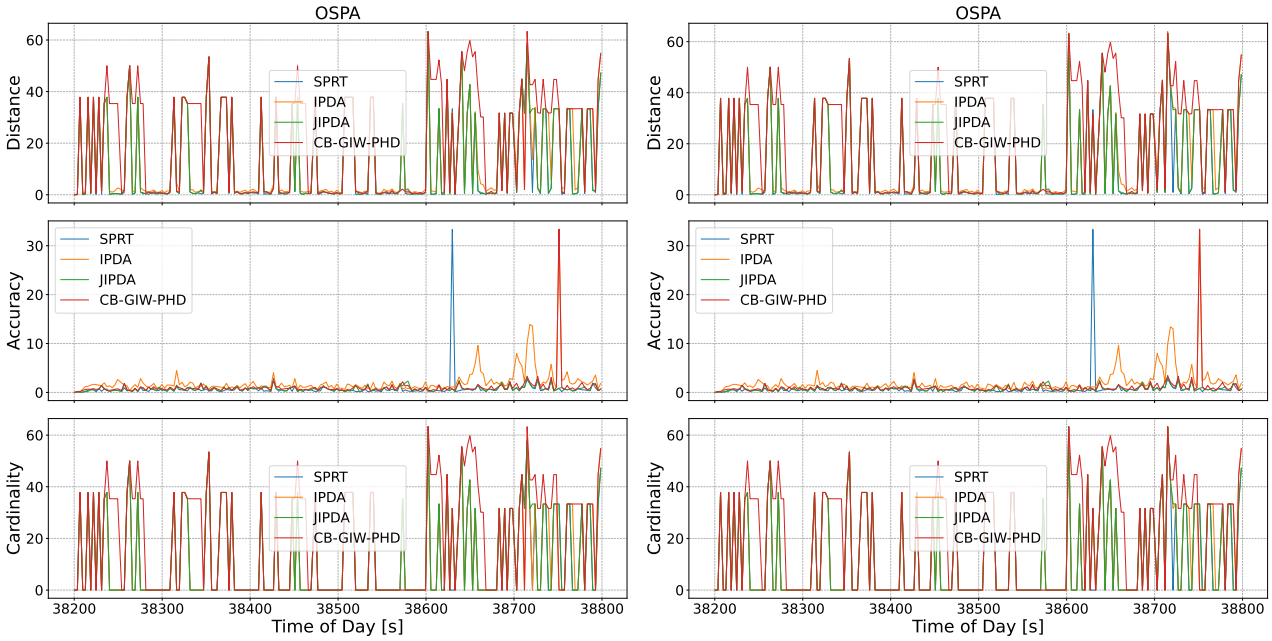

Fig. 3: OSPA metrics per frame for near-field scenario. Plots on the left are the trackers results for clustering in Cartesian domain. On the right the results for clustering in polar domain.

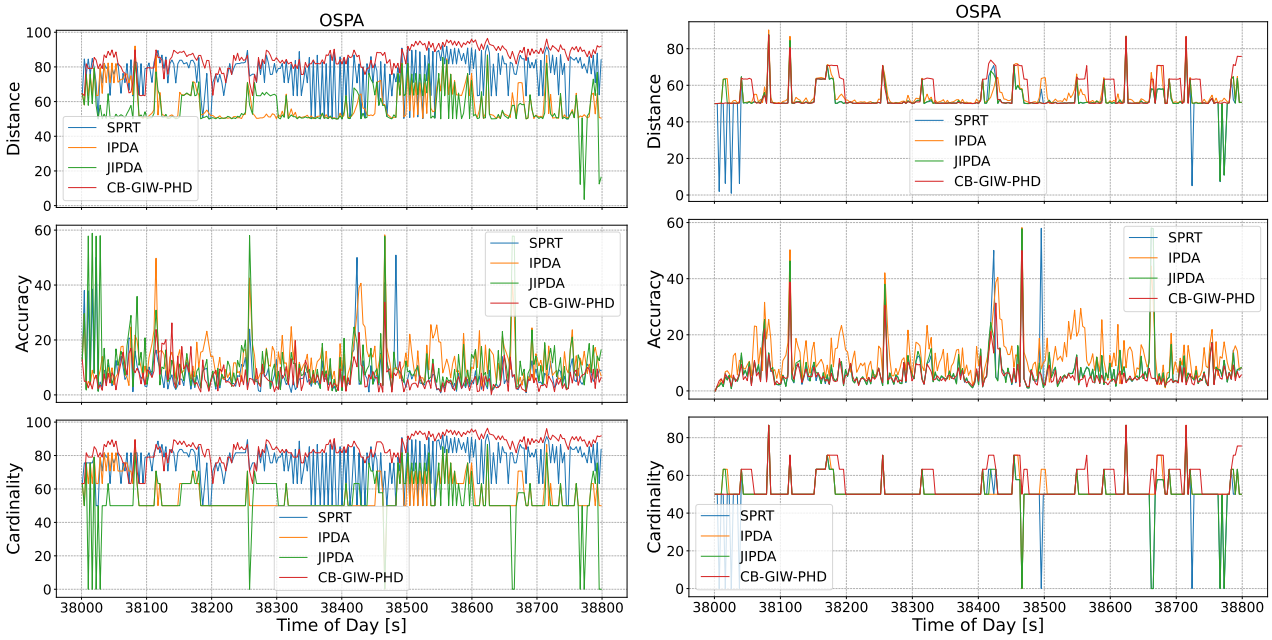

Fig. 4: OSPA metrics per frame for far-field scenario. Plots on the left are the trackers results for clustering in Cartesian domain. On the right the results for clustering in polar domain.

TABLE I: T-GOSPA Track Switching Cost

Scenario	Case	SPRT	P-IPDA	P-JIPDA	CB-GIW-PHD
Near Field	Cartesian	9.0	5.5	9.0	**3.5**
	Polar	9.0	5.5	9.0	**3.5**
Far Field	Cartesian	141.0	17.0	23.0	175.0
	Polar	5.0	3.5	4.0	**3.0**

behavior of the tracker, to fill misdetections caused by occlusion. An alternative approach would be to use targets positions from AIS messages as ground-truth reference, however non-collaborative vessels and AtoN objects would distort the metrics.

In the far-field ROI, where fewer spread measurements are detected, a smaller value of ε can make DBSCAN associate such detections as noise and no cluster is formed. In cases where more samples are available, the high spatial separation between them can make the algorithm to deliver more clusters for the same object. In the first case, the successive appearance and disappearance of objects leads to a high switch of track ID, as new tracks are proposed when new measurements are available, which can be seen in the results in Table I. The later can cause a higher amount of proposed tracks, generating a higher distortion in the cardinality results. In addition, a noticeably better performance of the PHD tracker can be explained by a different hypothesis generation logic, where reasonably all combinations of tracks and measurements are produced. However, while in PDA family (including SPRT) all association hypothesis are merged back in the moment reduction step (so that no new hypothesis are produced), in PHD tracker this is conditioned by the gate in the merging step and for strongly mismatching hypothesis larger number of objects can be generated. Moreover, PHD tracker uses far simpler track pruning strategy compared to complex combined pruning of SPRT/PDA trackers and this may also result in fundamental difference. These effects can be seen in Fig. 4.

IV. Summary

In this work, we presented a spatial data clustering approach for data represented in polar coordinates. The presented method was evaluated on the performance of different extended-objects MTT algorithms applied to real-world maritime X-band radar data. The proposed clustering method tackles the issues inherent to the polar data, especially the variance of point cloud spatial density w.r.t. the distance to the sensor, impacting the most sensitive hyper-parameter in density-based clustering algorithms such as DBSCAN.

The effectiveness of this method was assessed in four different MTT frameworks with different levels of complexity. Their performance corroborate the robustness assumption of polar-domain clustering. Additionally, the quantitative analysis of those trackers show that despite the leap in complexity when comparing the SPRT and the CB-GIW-PHD algorithms, the gain in performance has not the same rate when applying to maritime radar data.

Future work includes comparing the proposed method against other clustering algorithms, exploring more advanced MTT algorithms, such as CPHD and PMBM, and a deeper investigation on the their parametrization for the maritime specificities.

References

[1] J. Han, S. Y. Kim, and J. Kim, "Enhanced target ship tracking with geometric parameter estimation for unmanned surface vehicles," IEEE Access, vol. 9, pp. 39 864–39 872, 2021.

[2] M. Feldmann, D. Fränken, and W. Koch, "Tracking of extended objects and group targets using random matrices," IEEE Transactions on Signal Processing, vol. 59, no. 4, pp. 1409–1420, 2011.

[3] J. W. Koch, "Bayesian approach to extended object and cluster tracking using random matrices," IEEE Transactions on Aerospace and Electronic Systems, vol. 44, no. 3, pp. 1042–1059, 2008.

[4] K. Granström, A. Natale, P. Braca, G. Ludeno, and F. Serafino, "Gamma gaussian inverse wishart probability hypothesis density for extended target tracking using x-band marine radar data," IEEE Transactions on Geoscience and Remote Sensing, vol. 53, no. 12, pp. 6617–6631, 2015.

[5] G. Vivone, P. Braca, K. Granström, A. Natale, and J. Chanussot, "Converted measurements bayesian extended target tracking applied to x-band marine radar data," Journal of Advances in Information Fusion, vol. 12, no. 2, pp. 189–210, 2017.

[6] J. S. Fowdur, M. Baum, F. Heymann, and P. Banyś, "An overview of the pakf-jpda approach for elliptical multiple extended target tracking using high-resolution marine radar data," Remote Sens., vol. 15, no. 10, p. 2503, 2023.

[7] A. Fahim, "Adaptive density-based spatial clustering of applications with noise (ADBSCAN) for clusters of different densities," Computers, Materials and Continua, vol. 75, no. 2, pp. 3695–3712, 2023.

[8] V. Mistry, U. Pandya, A. Rathwa, H. Kachroo, and A. Jivani, "AEDBSCAN—adaptive epsilon density-based spatial clustering of applications with noise," in Progress in Advanced Computing and Intelligent Engineering, vol. 1199, 2020, pp. 213–226.

[9] X. Sun and P. Sajda, "Circular clustering with polar coordinate reconstruction," IEEE/ACM Transactions on Computational Biology and Bioinformatics, vol. 21, no. 5, pp. 1591–1600, 2024.

[10] EUROCONTROL Specification for Surveillance Data Exchange - ASTERIX Category 240: Radar Video Transmission, EUROCONTROL Std. 978-2-87 497-028-3, Rev. 1.3, 5 2015.

[11] S. Blackman and R. Popoli, Design and Analysis of Modern Tracking Systems. Artech House, 1999.

[12] T. Fortmann, Y. bar shalom, and M. Scheffe, "Sonar tracking of multiple targets using joint probabilistic data association. ieee journal of oceanic engineering, oe-8, 173-184," Oceanic Engineering, IEEE Journal of, vol. 8, pp. 173 – 184, 08 1983.

[13] Y. Bar-Shalom, F. Daum, and J. Huang, "The probabilistic data association filter," IEEE Control Systems Magazine, vol. 29, no. 6, pp. 82–100, 2009.

[14] D. Musicki and R. Evans, "Joint integrated probabilistic data association - jipda," in Proceedings of the Fifth International Conference on Information Fusion. FUSION 2002. (IEEE Cat.No.02EX5997), vol. 2, 2002, pp. 1120–1125 vol.2.

[15] D. Musicki, R. Evans, and S. Stankovic, "Integrated probabilistic data association," IEEE Transactions on Automatic Control, vol. 39, no. 6, pp. 1237–1241, 1994.

[16] D. Clark and B.-N. Vo, "Convergence analysis of the gaussian mixture phd filter," IEEE Transactions on Signal Processing, vol. 55, no. 4, pp. 1204–1212, 2007.

[17] K. Granström and U. Orguner, "On the reduction of gaussian inverse wishart mixtures," in 2012 15th International Conference on Information Fusion, 2012, pp. 2162–2169.

[18] J. M. Santos, , and M. Embrechts, "On the use of the adjusted rand index as a metric for evaluating supervised classification," in Artificial Neural Networks – ICANN 2009, vol. 2, 2009, pp. 175–184.

[19] D. Schuhmacher, B.-T. Vo, and B.-N. Vo, "A consistent metric for performance evaluation of multi-object filters," IEEE Transactions on Signal Processing, vol. 56, no. 8, pp. 3447–3457, 2008.

[20] Ángel F. García-Fernández, J. Gu, L. Svensson, Y. Xia, J. Krejčí, O. Kost, and O. Straka, "Gospa and t-gospa quasi-metrics for evaluation of multi-object tracking algorithms," 2025. [Online]. Available: https://arxiv.org/abs/2507.13706